C2H-

Benjamin A. Laws,[*,†,‡] Zachariah D. Levey,[†] Timothy W. Schmidt,[†] and Stephen T. Gibson[‡]

†*School of Chemistry, University of New South Wales, Sydney NSW 2052, Australia*

‡*Research School of Physics, The Australian National University, Canberra ACT 2601, Australia*

E-mail: b.laws@unsw.edu.au

Abstract

Introduction

Carbon monohydrides $C_{2n}H$, are a class of linear radicals that play an important role in combustion and interstellar chemistry. These carbon chains have been observed in many interstellar environments, including planetary atmospheres, comets, dark clouds, and during heavy star formation. Due to their relatively high abundance in a variety of astronomical conditions, they have been proposed to be promising candidates for Diffuse Interstellar Band carriers. The corresponding anions $C_{2n}H^-$ are also believed to play an important role in interstellar chemistry. C_6H^- was the first negative ion detected in space, after it was observed in the circumstellar envelope of IRC+10216 in 2006. More recently, anions C_4H^- and C_8H^- have also been detected in a range of environments, include dark clouds, prestellar cores, and prostellar envelopes.

Chain growth of the $C_{2n}H$ radicals occurs predominately through acetylene addition,

$$C_{2n}H + C_2H_2 \rightarrow C_{2n+2}H + H_2. \tag{1}$$

Conversely, the formation of anions in space is believed to be driven by radiative electron attachment, charge transfer, and dissociate electron attachment. However modelling these processes underestimates the abundance of C_4H^- observed in IRC+10216. Therefore, ion-neutral reactions have been proposed as an additional chain growth mechanism that also needs to be considered,

$$C_{2n}H^- + C_2H_2 \rightarrow C_{2n+2}H^- + H_2. \tag{2}$$

Modelling of the extraterrestrial planetary atmosphere of Saturn's moon Titan, suggests that both C_2H and C_2H^- play an important role in the atmospheric chemistry. Multiple reaction

pathways were included for the ion C_2H^- including,

$$C_2H^- \xrightarrow{H^+} C_2H_2 \tag{3}$$

$$\xrightarrow{HCN} CN^- + H_2 \tag{4}$$

$$\xrightarrow{C_2H_2} C_4H^- + H_2 \tag{5}$$

$$\xrightarrow{C_2H_2} C_4^- + H_3. \tag{6}$$

Understanding interstellar chemistry relies critically on theory, to provide a link between astronomical observations and terrestrial laboratory studies. Microwave spectroscopy has successfully been used in this fashion to identify a large number of molecules in the ISM. However for some species, particularly those with low abundances, UV/vis spectroscopic methods are required for identification. This creates a challenge for theory, as electronic spectra calculations are a lot more sensitive to the level of theory employed than pure rotational spectra. This becomes even more challenging when vibronic coupling effects are introduced, as they can be exceedingly difficult to model.

These considerations may be explored by examining some of the smallest carbon monohydrides. The ethynyl radical C_2H may appear to be a simple linear triatomic molecule. However the electronic spectrum is complicated by the presence of the close-lying ground $^2\Sigma^+$ and first excited $^2\Pi$ surfaces, which are only separated by $\sim 4,000$ cm^{-1}. The interaction of these surfaces produces a complex vibronic spectrum around the $\tilde{A}^2\Pi$ origin, where no single band corresponding to the $\tilde{X} - \tilde{A}$ origin has been observed. In C_4H the $^2\Sigma^+$ and $^2\Pi$ states are nearly degenerate, resulting in even stronger coupling, while in C_6H and C_8H the ordering of the states swaps, with a ground $^2\Pi$ state and a low lying excited $^2\Sigma^+$ state. Consequently, understanding these vibronic coupling interactions between the $^2\Sigma$ and $^2\Pi$ surfaces will be essential in order to accurately model the role these radicals (and their corresponding anions) are likely to play in the interstellar chemistry mentioned above, and to discern if they may be possible DIB carriers.

In this paper we study the vibronic spectrum of the ethynyl radical C_2H by employing High-Resolution Photoelectron Imaging (HR-PEI) in order to benchmark CFOUR *ab-initio* vibronic-coupling calculations. C_2H is reported to be one of the most abundant molecules in the universe, and is the most thoroughly studied of the $C_{2n}H$ species. Many different experimental techniques have been employed to try and resolve the complex vibronic spectrum, including electron spin resonance, laser magnetic resonance, microwave and milli-meter wave spectroscopy, infrared (matrix isolation and Fourier Transform) spectroscopy, and photoelectron spectroscopy. Extensive theoretical work on C_2H has also been carried out, in order to try and decode the surprisingly complex spectra that are observed in the experimental studies, however this has proven to be far from straightforward. In this work we demonstrate how the procedures set out in CFOUR may be used to calculate the strength of the vibronic interaction between coupled surfaces near a conical intersection, in order to simulate electronic and vibronic spectra. By employing anion HR-PEI both the $^2\Sigma^+$ and $^2\Pi$ surfaces are mapped out on an equal footing from the anion $\tilde{X}^1\Sigma^+$ state, allowing for direct comparison to the *ab-initio* modelling.

Results and Analysis

Ethynyl ions were produced in a pulsed-jet discharge of pure C_2H_4 gas, and subsequently mass isolated via time of flight. Electrons were detached using a tuneable Sunlite Optical Parametric Oscillator (OPO) pumped with the third harmonic of a Nd:YAG laser. High electron counts could also be obtained by using the third and fourth harmonics of the Nd:YAG laser directly. The detached electrons were then mapped onto a micro channel plate detector using a Velocity Map Imaging (VMI) lens. An illustrative VMI of ∼4 million electrons collected from 355 nm (3.49 eV) photodetachment of C_2H^- is shown in Fig. 1(a). The electrons are distributed radially according to their speed, with slow electrons at the image center, and fast electrons located towards the outer edge. Due to the relatively large C_2H^- elec-

tron affinity (EA) of 2.969 eV,[1] photodetachment at 355 nm occurs close to threshold. This yields slow electrons, allowing for a low repeller voltage (−600 V) on the VMI lens, and high velocity resolution.

Despite being close to threshold, two electronic states of neutral C_2H are observed. The faster electrons on the outer edge correspond to $C_2H(\tilde{X}\,^2\Sigma^+) + e^- \leftarrow C_2H^-(\tilde{X}\,^1\Sigma^+) + h\nu$ photodetachment, and are preferentially distributed around the poles of the image, indicative of a positive anisotropy parameter. Conversely the angular distribution of the slower electrons near the center are skewed towards the equator, indicative of a negative anisotropy parameter. These electrons may be assigned to photodetachment to the first excited state $C_2H(\tilde{A}\,^2\Pi) + e^- \leftarrow C_2H^-(\tilde{X}\,^1\Sigma^+) + h\nu$.

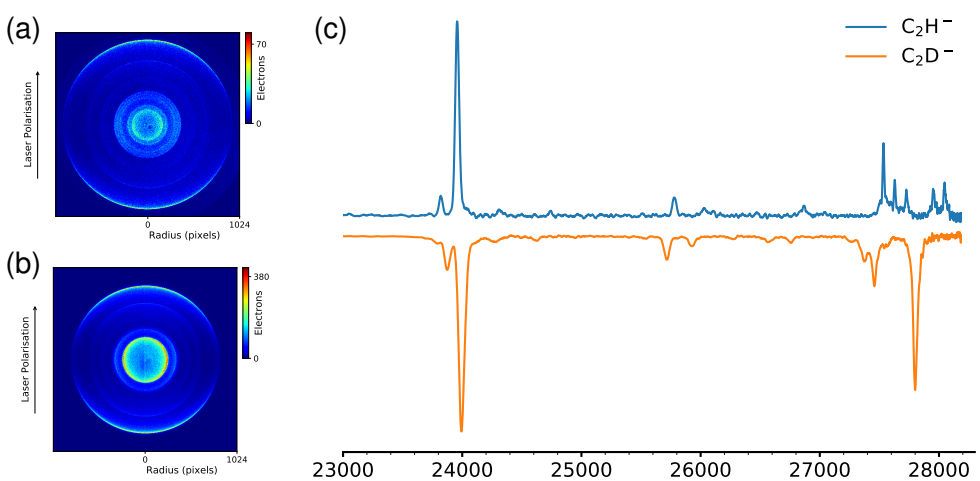

Figure 1: (a) A 3D-representation of the velocity-map image of ∼ 4 million photoelectrons detached from C2H$^-$ at 355 nm. The outer rings, distributed around the vertical laser polarisation axis, represents photodetachment to the ground $\tilde{X}\,^2\Sigma^+$ state. The inner rings reprsent detachment to the first excited state $\tilde{A}\,^2\Pi$. (b) Photoelectron spectra of C_2H^- at a range of detachment wavelengths, illustrating the change in electron intensity profile and energy resolution.

To investigate the vibronic coupling interaction between these two nearby Σ^+ and Π surfaces, deuterated ethynyl C_2D^- was also studied. C_2D^- ions were produced in a discharge of pure C_2D_4 gas and measured under the same experimental conditions as C_2H^-. An illustrative VMI of photodetachment at 355 nm from C_2D^- is shown in Fig. 1(b). Similarly to

Fig 1(a) two electronic states are observed - fast electrons with a positive anisotropy corresponding to detachment to the $^2\Sigma^+$ surface, and slow electrons with a negative anisotropy corresponding to $^2\Pi$ detachment. While the fast electrons appear similar in both images, a striking difference is observed in the slow electrons near the detector center. In Fig. 1(a) a series of weak rings are observed, however in Fig. 1(b) two dominant rings are seen.

The VMI in Fig. 1 were inverted using the Abel inversion methods detailed in pyAbel, to extract the corresponding photoelectron spectra, which are presented in Fig. 1(c). Below $27,000$ cm^{-1} the C_2H^- and C_2D^- spectra appear very similar. Both are dominated by the origin transition, shifted by ~ 10 cm^{-1} in the deuterated spectrum, and show a progression in the 2_0^{n+1} and $3_0^1 2_0^{n+1}$ vibrational modes. Within the harmonic oscillator approximation, transitions involving an odd quanta of vibrational excitation in the non-symmetric $v_2(\pi)$ mode should be totally forbidden. However, their presence in the photoelectron spectrum in Fig. 1(c) is likely an indicator of Herzberg-Teller (HT) vibronic coupling between the ground $^2\Sigma^+$ and nearby excited $^2\Pi$ electronic surfaces, as

$$\Sigma^+ \otimes \pi = \Pi. \tag{7}$$

Above $27,000$ cm^{-1}, near the $\tilde{A}^2\Pi$ state origin, large differences are observed between the C_2H^- and C_2D^- photoelectron spectra in Fig. 1(c). In the C_2H^- spectrum 5 sharp peaks are observed, spaced by ~ 95 cm^{-1}. However in the deuterated spectrum, one dominant peak is observed at $27,792$ cm^{-1}, with 3 weaker peaks centred around $27,360$ cm^{-1}. Unlike the structure below $27,000$ cm^{-1} none of these peaks are able to be readily assigned to vibronic transitions, due to the presence of strong coupling interactions between the nearby Σ^+ and Π surfaces.

Vibronic Coupling Interactions

The surprisingly complex spectral structure observed near the $\tilde{A}^2\Pi$ state origin in the photoelectron spectra in Fig. 1(c), may be understood by considering the v_2 bending vibrational mode. To account for the degeneracy of this mode we may introduce the vibronic quantum number ℓ_i, representing the angular momentum associated with the bending motion. This may take a value of $\ell_i = v_i, v_i - 2, v_i - 4, \ldots, 1$ or 0, where v_i is the quanta of bending excitation. In the Born-Oppenheimer approximation different vibronic energy levels ℓ_i are degenerate, however in cases with strong rovibronic coupling, this degeneracy in ℓ_i is lost.

In C_2H this effect creates a Renner-Teller (RT) pair in the excited state, where the usually degenerate Π surfaces separate to form two non-degenerate electronic states $\Pi^+(2A')$ and $\Pi^-(1A'')$. This involves separating a single potential energy surface (V) into two distinct but connected surfaces (V^+) and (V^-). Due to the strong coupling along the linear axis between the electronic and vibration angular momenta of the $2A'$ and $1A''$ components of the $^2\Pi$ state, stationary states cannot be explicitly assigned to either of the $\Pi^+(2A')$ or $\Pi^-(1A'')$ electronic surfaces. Instead, they exist as a combination of both states.

Due to the close lying nature of the ground $\tilde{X}^2\Sigma^+$ and excited $\tilde{A}^2\Pi$ electronic states, which are only separated by ~ 3700 cm^{-1}, a pseudo Jahn-Teller effect is also observed. The Jahn-Teller theorem states that stability and degeneracy are not possible simultaneously unless the molecule is linear,[2] meaning that non-linear molecules with degenerate electronic states will undergo a symmetry breaking distortion in order to remove the degeneracy. However a similar effect has also been observed where coupling exists between a non-degenerate state and a nearby pair of degenerate states, even if a molecule is linear.

In the case of ethynyl this is seen as coupling between the ground $\Sigma^+(1A')$ and excited $\Pi^+(2A')$ states, induced by the bending motion of v_2. The ground state only couples to one of the Renner-Teller pair $\Pi^+(2A')$, as the other state $\Pi^-(1A'')$ has incorrect symmetry. This results in a very complex vibronic structure for the $\tilde{A}^2\Pi$ electronic state, with contributions from three coupled surfaces $\Sigma^+(1A')$, $\Pi^+(2A')$, and $\Pi^-(1A'')$.

These interactions spread the electronic orgin of the $\tilde{A}\,^2\Pi$ state over several vibronic levels. Therefore, instead of assigning a defined origin, the observed peaks in the spectrum may be assigned to coupled admixtures of vibronic transitions involving the three potential energy surfaces,

$$\Psi_f = \sum_{\xi} \psi_e^{\xi} \sum_{k} C_{fk}^{\xi} \phi_{fkm}^{\xi}, \tag{8}$$

where ψ_e^{ξ} is the diabatic electronic wavefunction, and ϕ_{fkm}^{ξ} is the spin-rovibrational wavefunction. ξ represents the electronic states used in the expansion, and in this case $\xi = \Sigma^+(1A'),\ \Pi^+(2A'),\ \Pi^-(1A'')$. A depiction of these three interacting surfaces is given in Fig. 2.

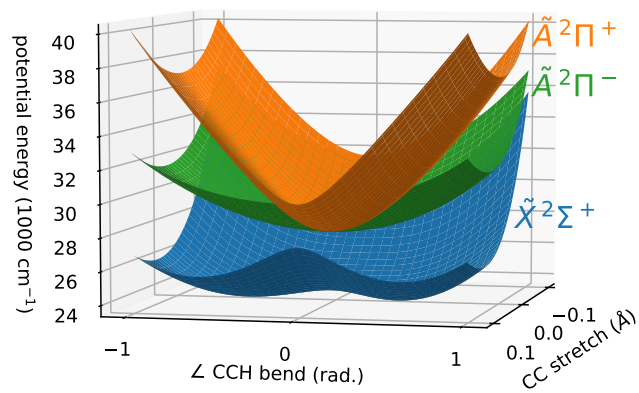

Figure 2: Adiabatic potential energy surfaces of $\tilde{X}^2\Sigma^+$, $\tilde{A}^2\Pi^-$, and $\tilde{A}^2\Pi^+$ states, calculated using the method developed by Tarroni and Carter[3] ($E_{1A'}$, $E_{2A'}$, and $E_{1A''}$ in Eq. 8).

Tarroni and Carter[3] have demonstrated that a large number of admixed vibronic levels may be calculated using the potential energy surfaces in Fig. 2. In fact, over 100 vibronic levels have been calculated, upto 6,400 cm^{-1} above the $\tilde{X}$ state origin. However assigning these levels to experimental spectra has remained a challenge, partly due to the large number of calculated vibronic levels, and partly due to the resolution of the experimental data in the literature.

Photoelectron Angular Distributions

Symmetry considerations can be employed to help assign the admixed structure in the experimental photoelectron spectra around the $\tilde{A}^2\Pi$ origin. As the detachment laser is linearly polarized, the angular distribution of the electrons in Fig. 1 may be linked to the symmetry of the detachment orbital. For polarised light, the differential cross section is given by

$$\frac{\mathrm{d}\sigma}{\mathrm{d}\Omega} = \frac{\sigma_{\mathrm{total}}}{4\pi}[1 + \beta P_2(\cos\theta)], \tag{9}$$

where θ is the angle between the ejected electron and the (vertical) laser polarization, and P_2 is the second-order Legendre polynomial. The anisotropy parameter β provides a quantitative measure of the angular distribution, and can range from -1 to +2 for a pure parallel and perpendicular transition respectively.** From Eq. (9), β may be determined for each transition in a photoelectron spectrum from the slope of I(θ) vs $P_2(\cos\theta)$. Through conservation of angular momentum, it can be shown that β may also be expressed in terms of partial waves and dipole matrix elements. Explicitly,

$$\beta_\ell = \frac{[\ell(\ell-1)\chi^2_{\ell,\ell-1} + (\ell+1)(\ell+2)\chi^2_{\ell,\ell+1} - 6\ell(\ell+1)\chi_{\ell,\ell-1}\chi_{\ell,\ell+1}\cos\delta_{\ell+1,\ell-1}]/(2\ell+1)}{\ell\chi^2_{\ell,\ell-1} + (\ell+1)\chi^2_{\ell,\ell+1}}, \tag{10}$$

where ℓ is the electron orbital angular momentum of the parent anion orbital, $\chi_{\ell,\ell\pm1}$ is the radial dipole matrix element for the transition from an orbital ℓ to each of the $\ell \pm 1$ partial waves, and $\delta_{\ell+1,\ell-1}$ is the phase shift between the two $(\ell \pm 1)$ partial waves.

As the radial dipole matrix elements will vary with electron kinetic energy, so too will β. Therefore, measuring anisotropy parameters at a range of energies will reveal the character of the detachment orbital. Anisotropy parameters were calculated for all resolved transitions in the C_2H^- photoelectron spectra from $266 - 355$ nm, and for C_2D^- at 355 nm ,as shown in Fig. 3.

Photodetachment to the ground state of C_2H^- ($\tilde{X}\,^1\Sigma^+$) involves ejecting an electron from

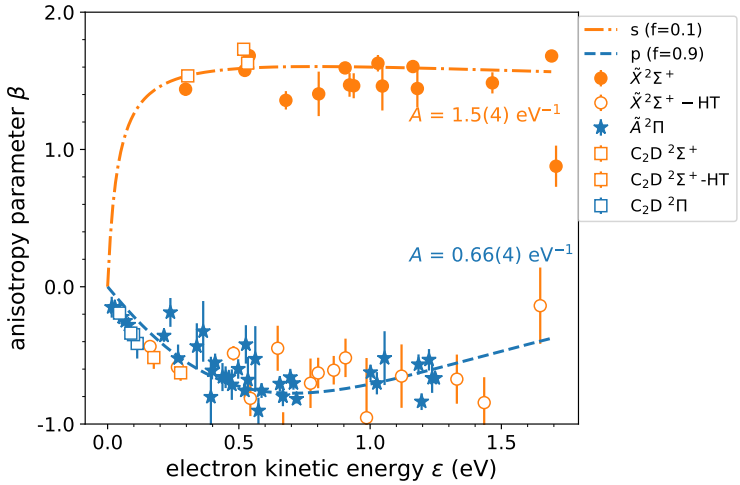

Figure 3: cat

an $s-$like $5\sigma_g$ orbital, whereas detachment to the excited ($\tilde{A}\,^2\Pi$) state occurs from a $p-$like $1\pi_u$ orbital. For a pure s and p orbital, the energy dependence of the anisotropy parameter may be described by Equations (11) and (12) respectively,

$$\beta_s = 2, \tag{11}$$

and,

$$\beta_p = \frac{2\mathrm{A}_1^2\epsilon^2 - 4\mathrm{A}_1\epsilon\cos\delta_{2,0}}{1 + 2\mathrm{A}_1^2\epsilon^2}, \tag{12}$$

where the Hanstorp coefficient A_1 relates to the ratio of radial matrix elements $\frac{\chi_{1,2}}{\chi_{1,0}}$ and $\delta_{2,0}$ represents the partial wave phase shift. As molecular orbitals may not be pure, we can describe the detachment from C_2H^- using the mixed sp model of Sanov,[4]

$$\beta(\epsilon)_{sp} = \frac{2Z\epsilon + 2\mathrm{A}_1\epsilon^2 - 4\epsilon\cos\delta_{\ell\pm1}}{\frac{1}{\mathrm{A}_1} + 2\mathrm{A}_1\epsilon^2 + Z\epsilon} \tag{13}$$

where f is the percentage of p character of the orbital,

$$Z = \frac{1-f}{f}\frac{8}{3} \quad \text{and} \quad |\psi\rangle = \sqrt{1-f}|s\rangle + \sqrt{f}|p\rangle. \tag{14}$$

Equation (13) may be fitted to the experimental anisotropy parameters in Fig. 3 to determine the orbital character and Hanstorp coefficients. All transitions to the $\tilde{A}^2\Pi$ surface may be described by detachment from an orbital with 90% s character, and a Hanstorp coefficient of A=1.5(4) eV^{-1}. However describing transitions to the $\tilde{X}^4\Sigma^+$ surface is complicated by the presence of HT coupling, which allows for the electronic character of two surfaces to be mixed via the promoting v_2 mode. The non-coupled allowed transitions may be described by detachment from an orbital with 90% p character, and a Hanstorp coefficient of A=0.66(4) eV^{-1}. However the forbidden 2^{2n+1} transitions follow the s-like detachment of the excited state. Therefore, measuring the anisotropy parameter of transitions near the conical intersection, where transitions to both surfaces overlap, will determine the symmetry of each level. This can then be compared to the calculated vibronic levels of Ref.** to help assign the transitions, as shown in Table S1 and S2.

Coupling Calculations

In order to investigate the role of $C_{2n}H$ and $C_{2n}H^-$ species in interstellar chemistry, theoretical approaches are required to link the terrestrial laboratory studies to astronomical observations. In particular, the ability to simulate electronic absorption spectra under interstellar conditions is required to survey potential DIB carriers. However the strong vibronic coupling in $C_{2n}H$ species that has been explored in this study, makes these calculations exceedingly difficult.

Here, we show how the photoelectron spectrum of C_2H^-, including vibronic coupling effects, may be simulated using a quasidiabatic Hamiltonian. Complications brought about by the vibronic interactions between the strongly coupled Σ^+ and Π states in the adiabatic representation can be avoided - in principle - via a transformation to a diabatic model. A useful diabatic nuclear kinetic energy operator may be achieved by representing the wavefunction of the molecule as a product of the electronic wavefunction with electronic coordinates at a

frozen reference geometry, and vibrational wavefunction

$$\Psi_{\text{diabatic}} = \psi_0 \chi. \tag{15}$$

The electronic states responsible for the failure of the adiabatic model may be isolated (in the diabatic basis) from the rest of the electronic states (in the adiabatic basis). This mixing of states prevents the electronic Hamiltonian from being strictly diagonal. However, if the frozen electronic states are well-chosen, then the off-diagonal terms in the kinetic energy operator are small and can be effectively neglected. This resulting electronic basis is the quasidiabatic representation.

$$\boldsymbol{V} = \begin{pmatrix} \Delta_0^X + \sum_i F_i^X q_i + \frac{1}{2}\sum_i F_{ij}^X q_i q_j & \sum_i \lambda_i^{XA} q_i \\ \sum_i \lambda_i^{AX} q_i & \Delta_0^A + \sum_i F_i^A q_i + \frac{1}{2}\sum_i F_{ij}^A q_i q_j \end{pmatrix}$$

The diagonal terms of $\boldsymbol{V}$ represent the quasidiabatic potential energy surfaces, and contain force constants F associated with the normal modes i,j. Δ_0 is the vertical electron detachment energy from C2H$^-$ to the neutral $\tilde{X}^2\Sigma^+$ ground state of C2H, denoted X, and the low-lying $\tilde{A}^2\Pi$ excited state, denoted A. The off-diagonal terms of $\boldsymbol{V}$ contain the coupling constants between the quasidiabatic electronic states, λ. The adiabatic potential energy surfaces, ν_x and ν_a, are obtained through the diagonalization of $\boldsymbol{V}$ and are equal to the quasidiabatic surfaces at a reference geometry, R_0. Additionally, this applies to all structures displaced from R_0 along totally symmetric coordinates, but loses this correspondence along coupling coordinates, particularly at a conical intersection. Therefore, all force constants in the diagonal blocks of $\boldsymbol{V}$ in the quasidiabatic representation that are associated with totally symmetric coordinates are equivalent to those obtained in the adiabatic representation and, thus, can be generated using standard ab initio quantum-chemical calculations.

$$F_i^X = \left(\frac{\delta\nu}{\delta q_i}\right)_{R_0}; \quad F_i^X = \left(\frac{\delta\nu^2}{\delta q_i \delta q_j}\right)_{R_0}; \quad ...$$

$$\forall i, j ... \in \Gamma_t ot.symm.,$$

For the case in which the normal modes, ij, correspond to coupling modes, the diabatic force constants F_{ij} and the adiabatic force constants are not equal due to the off-diagonal coupling terms, and are instead written

$$F_{ij}^{X(A)} = f_{ij}^{X(A)} + \frac{2\lambda_i \lambda_j}{\Delta_{X(A)}^{A(X)}}, \quad \Delta_B^A = E_A - E_X,$$

where F_{ij} and f_{ij} are the quasidiabatic and adiabatic force constants, respectively. Δ_X^A is equal to the vertical energy difference between the coupled states X and A at the reference geometry. Furthermore, due to the large geometrical differences between the reference and final states, force fields are not calculated at the reference geometry – on the adiabatic surface – but rather, are calculated at the minima of the final states and are transformed into the basis of the reduced normal coordinates of the reference state. This is known as "adiabatic parametrization", and is necessary to generate reasonable diabatic force constants.

Lastly, the off-diagonal terms of $\boldsymbol{V}$ are the coupling constants between the vibronically mixed final states and were determined analytically. ***Need John's help...Did we do any transformation to make PJT quasidiabatic...***

The adiabatic potential energy surfaces were calculated using the coupled cluster method with single, double and triple excitations (CCSDT). A restricted Hartree-Fock (RHF) reference function was used, along with the atomic natural orbital (ANO) basis set. The basis included...***help*** (ANO2). The geometries for each state were determined using a RHF-CCSDT/ANO2 optimization procedure based on analytic gradients. The quadratic force constants were calculated from harmonic frequency calculations based on analytic derivatives. The resulting coupling constants and force constants are presented in Table 1.

The resulting simulated spectrum is presented in Fig. **??** alongside the experimental photoelectron spectrum.

Discuss difference in C2H and C2D...

HT coupling allows for the electronic character of two surfaces to be mixed via a vibrational promoting mode. As shown in the Supplementary Materials, the transition dipole moment for a HT coupled transition may be rewritten as

$$\mu_{\alpha}^{a-n} = \langle \Psi_{\text{anion}} | \vec{\mu_{\alpha}} | \Psi_{\text{neutral}} \rangle \tag{16}$$

$$= \mu_{\alpha:0}^{\tilde{X}-\tilde{X}} \langle \chi''_{ms} | \chi'_{jt} \rangle + \gamma_{kr,jt} \mu_{a:0}^{\tilde{A}-\tilde{X}} \langle \chi''_{ms} | Q_n | \chi'_{kr} \rangle \tag{17}$$

where $\mu_{\alpha:0}^{\tilde{X}-\tilde{X}}$ and $\mu_{a:0}^{\tilde{A}-\tilde{X}}$ are the electronic transition moments for the $\tilde{X} \leftarrow \tilde{X}$ and $\tilde{A} \leftarrow \tilde{X}$ transitions, χ''_{ms}, χ'_{jt}, and χ'_{kr} are the nuclear components of the anion and neutral respectively, and $\gamma_{kr,jt}$ is the vibronic coupling constant. By comparing Eq. (17) to a Taylor series expansion of the transition dipole moment in Q_n about the anion equilibrium geometry, one can see that the vibronic coupling constant may be defined as,

$$\left(\frac{\partial \mu_{\alpha}^{\tilde{X}-\tilde{X}}}{\partial Q_n} \right)_0 = \gamma_{kr,jt} \mu_{a:0}^{\tilde{A}-\tilde{X}}. \tag{18}$$

Equation (18) shows that information about the vibronic coupling interaction between the neutral $\tilde{A} - \tilde{X}$ states may be obtained from determining the slope of the $\tilde{X} - \tilde{X}$ electronic transition moment along the vibrational promoting mode coordinate Q_n.

The resolution attainable using velocity-map imaging is dependent on the energy of the photoelectrons, $\Delta\epsilon \propto \epsilon$. Therefore, measurements close to threshold will provide the highest energy resolution, while shorter wavelength measurements will map a greater extent of the neutral vibrational structure. This variation is illustrated in Fig. 1(b), which shows the photoelectron spectra of C_2H^- resulting from photodetachment at 266 nm, 300 nm, 310 nm, 320 nm, and 355 nm. In the shorter wavelength measurements, spectral structure related to the $\tilde{A}\,^2\Pi$ state is observed up to 6000 cm^{-1} above the $\tilde{A}$ sate origin. A high resolution photoelectron spectrum of C_2H^- detachment at 355 nm extracted from a 2048×2048 image, similar to Fig. 1(a), via an inverse Abel transformation, is shown in Fig. **??**

Conclusions

Methods

Details of the HR-PEI spectrometer are given in Refs 5 and 6. CH_2CN^- ions are produced by passing a 1:1 C_2H_4:N_2O gas mixture through a pulse valve, which then undergoes supersonic expansion into a high-voltage discharge. Negative ions are extracted, accelerated to 500 eV, and focussed into a novel gating, bunching, and re-referencing unit.[7] Anions are mass separated over a 2m time-of-flight region, with the ion of interest isolated by an electrostatic gate. The ion packet is crossed with a tuneable detachment laser beam, generated from a Sunlite EX optical parametric oscillator pumped by the third harmonic of a Continuum Powerlite 9010 Nd:YAG laser. The laser produces between 10-50mJ per pulse at 10Hz, depending on whether the idler or signal beam is used. The wavelength of the laser light is measured using a HighFinesse WS7 UV wavemeter.

A velocity-map imaging lens, a modified version of the original concept of Eppink and Parker, images the detached electrons to a 75mm diameter MCP/phosphor screen detector. Events are imaged by a 2014x2048 monochrome CCD camera (PCO 2000), with each frame transferred to a computer at a 10Hz repetition rate, and processed in real time to identify individual electron events. The electron positions are centroided to a sub-pixel accuracy, then written to a data file for subsequent analysis. The velocity-map image is centred and then circularized by an angular dependent-radial scaling determined by comparing adjacent radial slice intensity profiles.[8] An inverse Abel transformation of the VMI, based on the algorithm of Hansen and Law,[9,10] returns a slice image of the 3D electron source distribution. Absolute energy calibration of the photoelectron spectra is achieved using published measurements of species, including O^-[5] and NO_2^-,[?] that have been studied under similar conditions as used for the CH_2CN^- measurements.

In standard operation, the energy distribution of the detached electrons is obtained by recording the velocity-mapped positions from photodetachment at a fixed wavelength. How-

ever the HR-PEI spectrometer may also be reconfigured into an electron counting mode, where the number of events per laser shot is recorded, while the detachment laser wavelength is varied.

Acknowledgement

This research was supported by the Australian Research Council Discovery Project Grants DP160102585 and DP190103151.

References

(1) Ervin, K. M.; Lineberger, W. C. Photoelectron spectra of dicarbon(1-) and ethynyl(1-). *The Journal of Physical Chemistry* **1991**, *95*, 1167–1177.

(2) Jahn, H. A.; Teller, E. Stability of polyatomic molecules in degenerate electronic states - I Orbital degeneracy. *Proceedings of the Royal Society of London A: Mathematical, Physical and Engineering Sciences* **1937**, *161*, 220–235.

(3) Tarroni, R.; Carter, S. Theoretical calculation of vibronic levels of C_2H and C_2D to 10âĂĽ000âĂĽcmâĹŠ1. *The Journal of Chemical Physics* **2003**, *119*, 12878–12889.

(4) Sanov, A. Laboratory-Frame Photoelectron Angular Distributions in Anion Photodetachment: Insight into Electronic Structure and Intermolecular Interactions. *Annual Review of Physical Chemistry* **2014**, *65*, 341–363.

(5) Cavanagh, S. J.; Gibson, S. T.; Gale, M. N.; Dedman, C. J.; Roberts, E. H.; Lewis, B. R. High resolution velocity-map imaging photoelectron spectroscopy of the O^- fine-structure transitions. *Physical Review A* **2007**, *76*, 052708.

(6) DeVine, J. A.; Weichman, M. L.; Laws, B.; Chang, J.; Babin, M. C.; Balerdi, G.;

Xie, C.; Malbon, C. L.; Lineberger, W. C.; Yarkony, D. R. et al. Encoding of vinylidene isomerization in its anion photoelectron spectrum. *Science* **2017**, *358*, 336–339.

(7) Dedman, C. J.; Roberts, E. H.; Gibson, S. T.; Lewis, B. R. Fast 1 kV metal-oxide-semiconductor field-effect transistor switch. *Review of Scientific Instruments* **2001**, *72*, 3718–3720.

(8) Gascooke, J. R.; Gibson, S. T.; Lawrance, W. D. A âĂIJcircularisationâĂİ method to repair deformations and determine the centre of velocity map images. *The Journal of Chemical Physics* **2017**, *147*, 013924.

(9) Hansen, E. W.; Law, P.-L. Recursive methods for computing the Abel transform and its inverse. *Journal of the Optical Society of America A* **1985**, *2*, 510–520.

(10) Hickstein, D. D.; Yurchak, R.; Das, D.; Shih, C.-Y.; Gibson, S. T. PyAbel (v0.7): A Python package for Abel transforms. https://github.com/PyAbel/PyAbel, 2016.